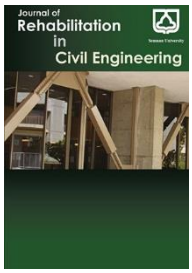

journal homepage: http://civiljournal.semnan.ac.ir/

Strengthening of Existing RC Two-Way Slabs using New Combined FRP fabric/rod Technique

P. Behzard[1*], M. K. Sharbatdar[2] and A. Kheyroddin[3]

1. Ph.D. In Structural Engineering, Faculty of Civil Engineering, Semnan University, Semnan, Iran.
2. Associate Professor, Faculty of Civil Engineering, Semnan University, Semnan, Iran.
3. Professor, Faculty of Civil Engineering, Semnan University, Semnan, Iran.
Corresponding author: pejmanb@gmail.com

ARTICLE INFO

Article history:
Received: 07 June 2015
Accepted: 27 February 2016

Keywords:
Combined FRP technique,
NSM GFRP rods,
EB CFRP fabrics,
RC two-way slabs,
Finite element.

ABSTRACT

This study presents the results of an experimental program to investigate the effectiveness of an innovative combined FRP technique using combination of externally bonded (EB) FRP fabrics and near surface mounted (NSM) FRP rods for flexural strengthening of existing reinforced concrete (RC) two-way slabs with low clear cover thickness. Three full-scale RC slabs (1500×1500×120 mm) were tested under monotonic four-point bending. One slab was kept un-strengthened as the control specimen, one slab was strengthened using NSM GFRP rods, and the other one slab was strengthened using combination of EB CFRP fabrics and NSM GFRP rods. The load-deflection responses, strain measurements, and failure modes of the tested slabs were studied and discussed. The behavior of the slab strengthened with this technique was compared to the behavior of the slab strengthened with GFRP rods. The test results confirmed the feasibility and efficacy of this technique in improving the flexural behavior of RC two-way slabs. Strengthened slabs showed an increase in flexural capacity between 250 and 394% over the control specimen. The slab strengthened using this technique showed higher ductility compared to the slab strengthened using GFRP rods. A 3D nonlinear numerical model was also developed using the finite element (FE) method to predict the flexural behavior of the tested slabs. A good agreement between experimental and numerical results was observed.

1. Introduction

Fiber reinforced polymer (FRP) reinforcements have been shown to be a proper option for strengthening of reinforced concrete (RC) structures. The main advantages of FRP materials for strengthening over traditional methods are

their high tensile strength to weight ratio, high fatigue strength, non-corroding, and high chemical resistance [1,2].

The near surface mounted (NSM) method is one of the latest strengthening techniques for RC structures. In this technique, grooves are cut into the surface of the concrete members; FRP reinforcements are inserted into the grooves and then bonded using epoxy or cement-based adhesive [3]. When compared to the externally bonded (EB) technique, the NSM technique assures a higher anchoring capacity to the FRP reinforcing material. Recently, De Lorenzis and Teng [4] provided a critical review of existing research on strengthening of structural members using the NSM FRP reinforcement technique. Over the past few years, extensive researches have been conducted on the NSM FRP reinforcement strengthening technique [5,6], and the results have shown the effectiveness of this technique in improving the flexural and shear behavior of RC structural members. However, most of the studies have focused on the strengthening of RC beams [7–10] or slab strips [11–15]. There are little experimental or analytical studies in the behavior of RC two-way slabs flexural strengthened with NSM FRP reinforcements.

The flexural capacity of RC two-way slabs can be increased by bonding the FRP rods or strips into grooves cut perpendicularly on the tension face. For two-way slabs, the NSM strengthening technique using the FRP reinforcement must be performed along two perpendicular directions. Foret and Limam [16] investigated experimentally the flexural behavior of RC two-way slabs with two strengthening techniques: NSM CFRP rods and EB CFRP strips. The experimental study consisted of three full-scale strengthened slabs in addition to one un-strengthened slab as the control specimen. It was concluded that the NSM technique improves the bearing capacity of RC two-way slabs. A more ductile behavior was also observed comparing to the EB technique. It was shown that, the specimen strengthened using EB CFRP strips experienced the premature debonding failure of the strips and carried approximately half the load carried by the specimen strengthened using NSM CFRP rods. However, it should be mentioned that conventional NSM technique can only be applied for slabs with sufficient clear cover thickness, because the grooves in one direction must be cut deeper than those in another direction. Therefore, this NSM strengthening technique is often limited, because the sufficient clear cover thickness is not available in most existing RC slabs. Furthermore, conventional EB technique is often limited in most slabs as well, due to the premature debonding failure of the EB FRP reinforcements from the concrete surface at low strain levels. To overcome these drawbacks, an innovative combined FRP technique for strengthening of existing RC two-way slabs through combination of EB CFRP fabrics and NSM GFRP rods is proposed in this study.

2. Research significance

This study investigates the feasibility and efficacy of an innovative combined FRP technique using combination of EB CFRP fabrics and NSM GFRP rods to increase the flexural capacity of existing RC two-way slabs with low clear cover thickness. To the authors' knowledge, the technique introduced in this study is the first investigation in the technical literature on the use of combined FRP technique for strengthening of the RC two-way slabs. An experimental program of four-point bending tests is carried out on the RC two-way slabs with a limited amount of internal steel reinforcements. To assess the effectiveness of this technique, a comparison is carried out between the behavior of the slab strengthened according to this technique and the behavior of the slab strengthened with conventional GFRP rods. A 3D nonlinear finite element (FE) simulation is also developed using

the FE code ANSYS [17] to predict the behavior of flexural strengthened slabs. The FE numerical predicted load-central deflection responses and failure modes are compared with that of the measured experimental results.

3. Experimental program

3.1. Material properties

Table 1 summarizes the material properties of the concrete, steel bars, FRP reinforcements, and epoxy used for test specimens. The average 28-day compressive strength of concrete from compressive cylinder tests was 24.82 MPa. The steel reinforcements were 10 mm diameter deformed steel bars with mean yield strength of 351.15 MPa obtained from uniaxial tension tests. The FRP reinforcements used in the strengthening application consisted of GFRP rods and flexible CFRP sheets. The rods used in this investigation were GFRP pultruded rods made of continuous E-glass fibers and vinyl-ester resin. The nominal diameter of the rods was 12 mm, and their surface was spirally ribbed. The sheets used in the strengthening application consisted of a custom stitched unidirectional carbon fabric. The thickness and width of the fabric was 0.13 and 500 mm respectively. The type and size of the FRP reinforcements was chosen based on commercial availability; however there was a good agreement between the axial stiffness of the different FRP materials used for test specimens. For bonding the FRP reinforcements to the concrete, Sikadur 30 structural epoxy paste adhesive was used, which is a two-component epoxy matrix material.

Table 1. Material properties.

Material	Elastic modulus (GPa)	Compressive strength (MPa)	Yield stress (MPa)	Yield strain (μstrain)	Ultimate tensile Stress (MPa)	Ultimate tensile strain (μstrain)
Concrete [a]	24.91	24.82	—	—	—	—
Steel [a]	200	—	351.15	2,160	520.85	159,332
GFRP rod [b]	60	—	—	—	1,000	15,000
CFRP fabric [b]	230	—	—	—	4,900	15,000
Sikadur 30 [b]	4.5	—	—	—	25	10,000

[a] Average values obtained from material testing.
[b] Values reported by the manufacturer.

3.2. Test specimens

Three full-scale RC two-way slab specimens were constructed with the same geometrical configuration and steel reinforcement details. The dimensions of the slabs were 1,500 mm long×1,500 mm wide×120 mm thick. The sides of the slabs represent the contra-flexure lines in an actual two-way slab system. The slabs were designed to obtain a pure flexural failure mode for the control specimen and possibly improve the flexural behavior of the strengthened specimens. The main flexural reinforcements (in one layer near the slab tension face) were 5-10 mm diameter deformed steel bars spaced at 300 mm along two perpendicular directions and arranged to give an average effective depth (d) to the center of the two layers of 80 mm. Thus, the clear cover thickness was about 30 mm. The reinforcement area provided in the slabs corresponded to reinforcement ratio of about 0.22%, which was close to the minimum reinforcement ratio for RC two-way slabs (0.2%), as specified by ACI 318-99 [18]. The anchorage of these bars was provided by 180 degree hooks at both ends. Figure 1 shows the layout of a test specimen and steel reinforcement details.

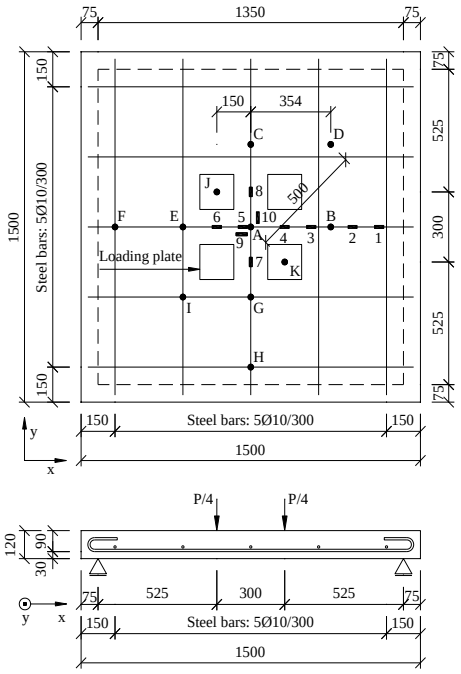

Figure 1. Test specimen layout and steel reinforcement details (all dimensions in mm).

3.3. Strengthening method

After curing, the specimens were rotated 180 degrees about their in-plane axis and placed on an elevated platform for strengthening. Out of the three specimens, one was kept un-strengthened as the control specimen. Control specimen simulates an existing RC slab requiring strengthening. The other two specimens were strengthened using different configurations of FRP reinforcements at the tension face of the slab. The amount and configuration of the FRP reinforcements was selected to provide a reasonable enhancement in the flexural capacity of the specimen. The specimens were named according to the different materials used for strengthening. The first and second phrases denoted the strengthening material in x and y directions respectively. The GFRP rod and CFRP fabric were denoted as R and F respectively. Therefore, the specimens were named as R-R and R-F. The specimen designation, description of FRP reinforcements and groove dimensions for specimens are given in Table 2.

Table 2. Specimen designation, FRP layout description and groove dimensions.

Specimen designation	Reinforcement material in x direction	Reinforcement material in y direction	Groove size in x direction b×h (mm)	Groove size in y direction b×h (mm)
Control	—	—	—	—
R-R	GFRP rod	GFRP rod	20×30	20×20
R-F	GFRP rod	CFRP fabric	30×20	—

The specimen R-R was strengthened using 4-12 mm diameter NSM GFRP rods in both x and y directions. The GFRP rods (1500 mm in long), spaced at 300 mm, were bonded into grooves on the slab tension face. When the concrete slabs attained, approximately, 28 days of age, eight grooves were cut into the concrete cover along two perpendicular directions on the tension face of the slabs. The grooves were spaced at 300 mm centers. A special concrete saw with a diamond blade was used to cut the grooves. For specimen R-R, the grooves in x direction were cut 10 mm deeper than those in y direction, as indicated in Table 2. The grooves were thoroughly cleaned of debris and dust using steel brushes and pressured air to ensure proper bonding between the epoxy adhesive and the concrete. Each groove was then half filled with the epoxy using a spatula, and the GFRP rods were subsequently inserted and lightly pressed. This forced the epoxy to penetrate around the rod and fill the space between the GFRP rod and the sides of the groove. At the grooves intersection, the GFRP rods, placed along two perpendicular directions, were passed on top of each other, as shown schematically in Figure 2(a). More epoxy was applied to fill the groove and the surface was leveled by removing the excess

adhesive. The specimen was cured for one week at room temperature before testing.

The specimen R-F was similarly strengthened in x direction using four NSM GFRP rods with the same arrangement as specimen R-R, but it used four EB CFRP fabrics as the strengthening reinforcements in y direction. For specimen R-F the grooves were cut in the same way as specimen R-R, except that the grooves were cut only in x direction, as indicated in Table 2. Before bonding the FRP fabrics, the slab face was roughened using wire brushes and then cleaned of all dirt by pressured air. The epoxy was then applied on the slab face using a spatula. The EB CFRP fabrics (1800 mm in length and 250 mm in width), spaced at 300 mm, were bonded on the slab tension face in y direction. At intersection with the grooves, the CFRP fabrics were folded into grooves and then bonded on the groove sides (Figures 2(b and c)). The grooves were then half filled with the epoxy and the GFRP rods were passed and bonded on top of the CFRP fabrics at those four portions which CFRP fabrics were bonded on the groove sides (Figure 2(d)), in order to prevent the separation of the EB GFRP fabrics from the groove sides. More epoxy was applied to fill the groove and the surface was leveled by removing the excess adhesive (Figures 2(e and f)). As a result, both of the GFRP rods and CFRP fabrics could be fit into the limited depth of the groove. All the FRP reinforcements were extended to the exterior edges of the slab to allow the utilization of a sufficient bond length of the FRP reinforcements. The specimens were cured for one week at room temperature before testing. Figures 3(a and b) shows a schematic layout of the three FRP strengthened specimens and FRP reinforcement details at the grooves intersection.

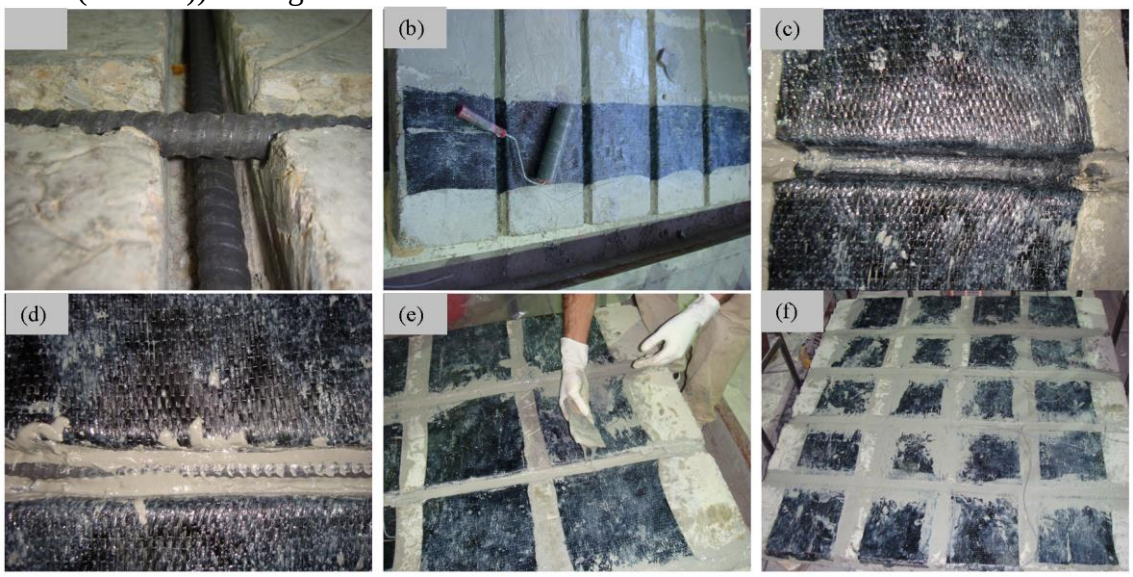

Figure 2. Strengthening process of slab specimens.

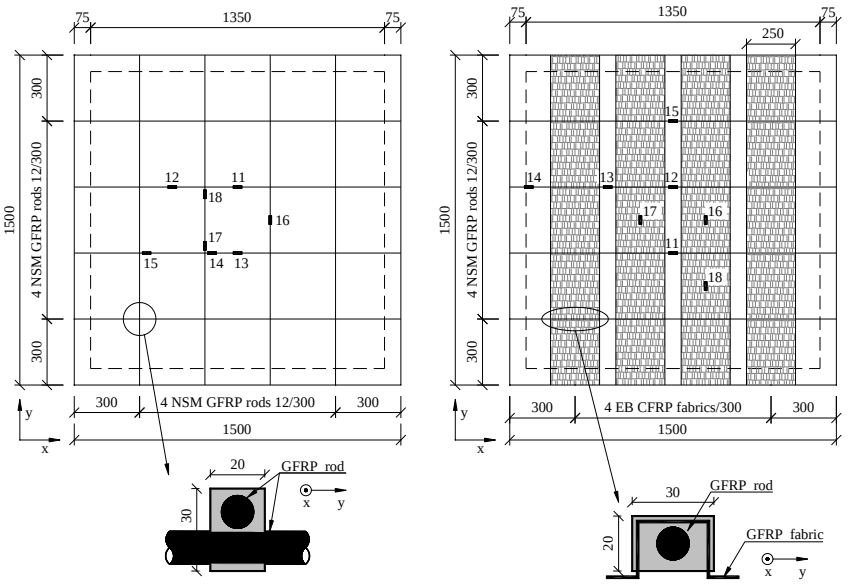

Figure 3. Schematic layout of strengthened specimens and FRP reinforcement details at the grooves intersection.

3.4. Test setup and instrumentation

The slabs were placed on a stiff supporting steel frame along their four sides. The stiff supporting frame rested on the strong concrete floor of the laboratory. Four steel rollers, 1350 mm apart on centre, were placed between the specimen four sides and the stiff supporting frame. This simulates the simply supports over the four edges of the specimen, thus permitting the corners free to uplift when load was applied. A stiff loading steel frame was used to test the specimens. All slabs were tested under monotonic load using a 500 kN hydraulic jack in four-point bending up to failure. The loading points and supports were selected to give an effective span of 1350 mm and a shear span of 300 mm in both directions, as shown in Figure 1. A cruciform spreader steel beam was used to transfer the load to the slab through four loading points. Four square steel loading plates (150×150×40 mm) were placed between the cruciform spreader beam arms and slab top face to avoid uneven application of the load. The load was gradually increased by successive 10 kN increments, which were progressively reduced near failure. The self-weight of the slab was small and neglected in the calculation of the applied loads. The test was stopped when the specimen failed.

The applied load was measured using a 500 kN load cell placed between the hydraulic jack and the stiff loading frame. The vertical deflection of the specimen was measured at eleven different locations using linear variable displacement transducers (LVDTs), denoted by points A to K in Figure 1. The LVDTs were attached on a stiff instrumentation steel frame placed below the slab bottom face and fixed at the base. One of the LVDTs was placed underneath the slab center to measure the central deflection of the specimen. Six LVDTs were placed along the orthogonal central lines to measure the deflection at 300, 345, and 600 mm away from the slab center. The other four LVDTs were placed along the diagonal lines at 212, 424, and 500 mm away from the slab center. Eight strain gauges, denoted as 1 to 8 in Figure 1, were bonded at different locations on the steel bars in each specimen. Concrete strains were also measured on the slab

compressive face along two perpendicular directions using two strain gauges, denoted as 9 and 10 in Figure 1. Based on the configuration of FRP reinforcements bonded on the slab tension face, eight gauges, denoted as 11 to 18 in Figures 3(a and b), were bonded on the FRP reinforcements at different locations. The locations of the strain gauges were selected in order to measure the maximum strains and to plot the strain distribution in the steel bars. Before bonding the gauges, the surface of the steel bars and GFRP rods were smoothed using an electrical disk sander and then cleaned with a solvent material. The readings from the load cell, LVDTs, and strain gauges were recorded by means of a data logger system. Figure 4 shows test setup and locations of the instruments.

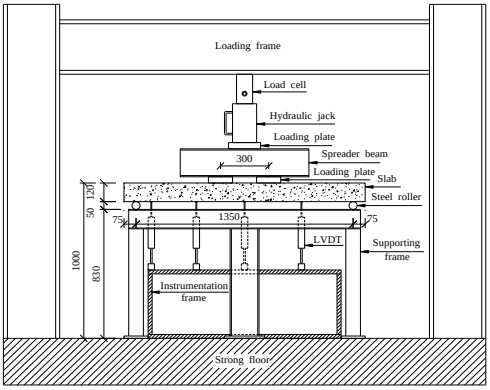

(a) Instrumentation

(b) Test setup

Figure 4. Test setup and locations of the instruments.

4. Test results and discussion

4.1. Load–deflection response

Table 3 summarizes the test results includingultimate load and deflection measurements for test specimens.

Figure 5 compares the load-central deflection response of all three test specimens. Central deflections shown in these plots represent central deflections relative to supports. The load-deflection response can be divided into un-cracked and cracked stages. The cracked stage also can be divided into pre-yield and post-yield sub-stages. The pre-yield cracked stage was from the cracking load (Pcr) to the yield load (Py). The post-yield cracked stage extended from the yield load (Py) to the ultimate load (Pu). The first cracking load can be accepted as the point where the load–deflection response deviated from the initial elastic response.

Table 3. Summary of test results.

Specimen	P_{cr} (kN)	P_y (kN)	P_u (kN)	Δ_{cr} (mm)	Δ_y (mm)	Δ_u [a] (mm)	% Increase in P_u with respect to Control	% Decrease in Δ_u with respect to Control	Displacement ductility (Δ_u/Δ_y)
Control	22.83	42.50	47.50	0.96	15.01	63.35	—	—	4.22
R-R	40.83	189.85	234.50	1.71	13.85	24.33	393.68	61.59	1.76
R-F	39.67	113.17	166.17	2.42	11.33	36.56	249.83	42.29	3.23

[a] Net central deflection at 20% drop of ultimate load carrying capacity.

A ductile failure was observed for control specimen. The load-deflection response of the control specimen consisted of a stiff un-cracked stage, followed by a yield plateau

due to yield of the steel bars. Yielding spread gradually from the slab center to the edges as the applied load increased which caused the formation of some yield lines. Finally, the specimen failed in pure flexural mode. The strengthened specimens exhibited combined flexural and local failure due to punching the loading plates through the slab. Failure took place after significant yielding of flexural reinforcement. As the applied load increased further, the regions near the loading plates entered into a plastic state, and the loading plates punched through the slab thickness. Punching the loading plates through the slab thickness at high load levels (between 3.50 and 4.94% times the ultimate load measured for the control specimen) is the nature of the four-point loading method in low thickness two way slabs and sometimes is unavoidable. For specimen R-R, failure occurred in a brittle manner and the load carrying capacity dropped abruptly. The specimen R-F presented more ductile behavior than the specimen R-R. For this specimen, failure occurred in a ductile manner and the load carrying capacity dropped gradually.

It can be seen by comparing the load-deflection responses of the specimens showed in Figure 5 and the ultimate load results presented in Table 3 that applying FRP reinforcements increased the cracking strength, flexural stiffness of the specimens, and resulted in considerable improvement in the flexural capacity. The corresponding increases depended on the area of the FRPs relative to the area of the conventional steel bars and the failure mode of the specimens. In addition, the load level at which the steel bars yielded (Py) depended on the FRP reinforcements area and configuration. The formation of yield lines was also influenced by the FRP reinforcements which tended to restrain the crack propagation.

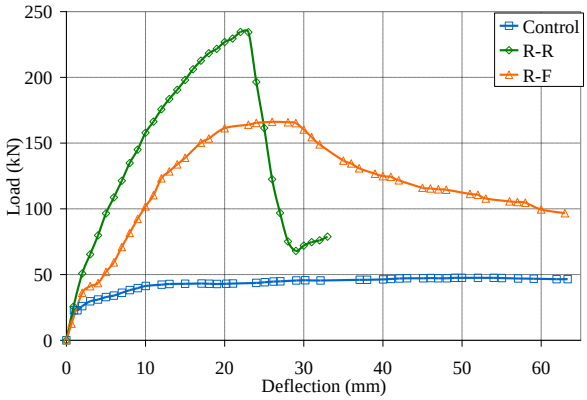

Figure 5. Comparison of load-deflection response of specimens.

4.2. Ultimate load and deflection

The control specimen experienced the lowest ultimate load (47.50 kN). The strengthened specimens had higher loading capacity than the control specimen. The specimen R-F had almost the increase in the ultimate load of 250 % over the control specimen. Specimen R-R, strengthened with GFRP rods, showed higher increase in the ultimate load, which was 394% over the control specimen. The control specimen had the highest deflection value (63.35 mm) at the corresponding ultimate load. Deflection values at the ultimate loads of the strengthened specimens were between 38 and 58% of the deflection value of the control specimen due to the stiffening effect of FRP reinforcements. Displacement ductility, defined as the ratio of deflection at the ultimate load divided by the deflection at first yield, were 4.22, 1.76, and 3.23 for specimens Control, R-R, and R-F respectively. Specimen R-F showed higher ductility compared to specimen R-R, but less ductility than the control specimen. It was shown that, the increase in flexural capacity was accompanied by a reduction in the ductility of failure.

4.3. Deflection profile

The deflection of the specimens at 0, 300, 345, and 600 mm away from the slab center

along the orthogonal axis and at 0, 212, 425, and 500 mm along the diagonal axis was measured continuously with increasing the applied load. At any load level, the highest deflection value was at the slab center, and deflections decreased with increasing the distance from the slab center. Figures 6 and 7 compare the deflection profiles of the control and strengthened specimens at the ultimate loads along the orthogonal and diagonal axis respectively. The control specimen had the highest deflection values at all locations among the test specimens. Specimen R-F had the highest deflection values among the strengthened specimens, but less deflection than the control specimen. Specimen R-R had the lowest deflection profile among the strengthened specimens.

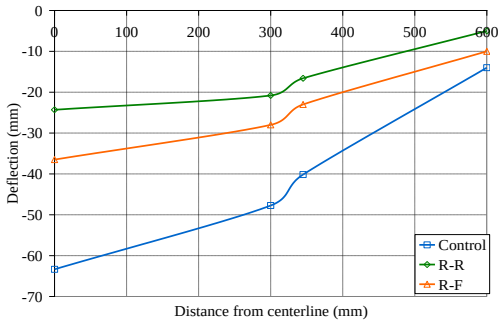

Figure 6. Deflection profile along the orthogonal axis at ultimate load.

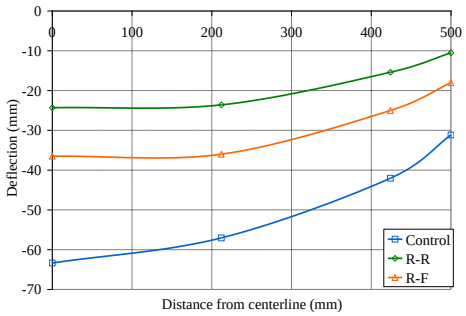

Figure 7. Deflection profile along the diagonal axis at ultimate load.

4.4. Cracking patterns and failure modes

Figure 8 shows the cracking patterns at the tension and compression faces of the specimens after failure. Control specimen failed in pure flexural failure mode by forming the flexural orthogonal yield lines at the slab tension face directly below the loading plates. Yield lines then extended from the corners of the loading plates in the diagonal direction and forked out as they approached the corners of the slab. There was no sudden loss of strength in the load-deflection response of the control specimen, although very large deflection was imposed. The failure of the control specimen was more ductile than those of the strengthened specimens, as indicated in Table 3. The strengthened specimens experienced combined flexural and local failure due to punching the loading plates through the slab in which both flexural yield lines and roughly circular cracks along the perimeter of the loading plates were observed to form simultaneously at failure. For strengthened specimens significant yielding was observed followed by the initiation of crushing of concrete around the loading plates.

All the strengthened specimens had smaller crack widths than the control specimen due to the effect of FRP reinforcements on restraining the crack propagation. It was observed that the load level at which failure occurred and the severity of failure of the specimens were influenced by the presence of the FRP reinforcements. The crack control provided by the FRP reinforcements was optimal when direction of the FRP reinforcements are oriented perpendicular to the crack. For specimen R-F, the developed tension in EB CFRP fabrics at high load levels tended to pull the GFRP rods out from the groove sides and hence caused debonding failure. As a result, the cracks distribution at the slab tension face were more concentrated in the x direction, where strengthened with GFRP rods.

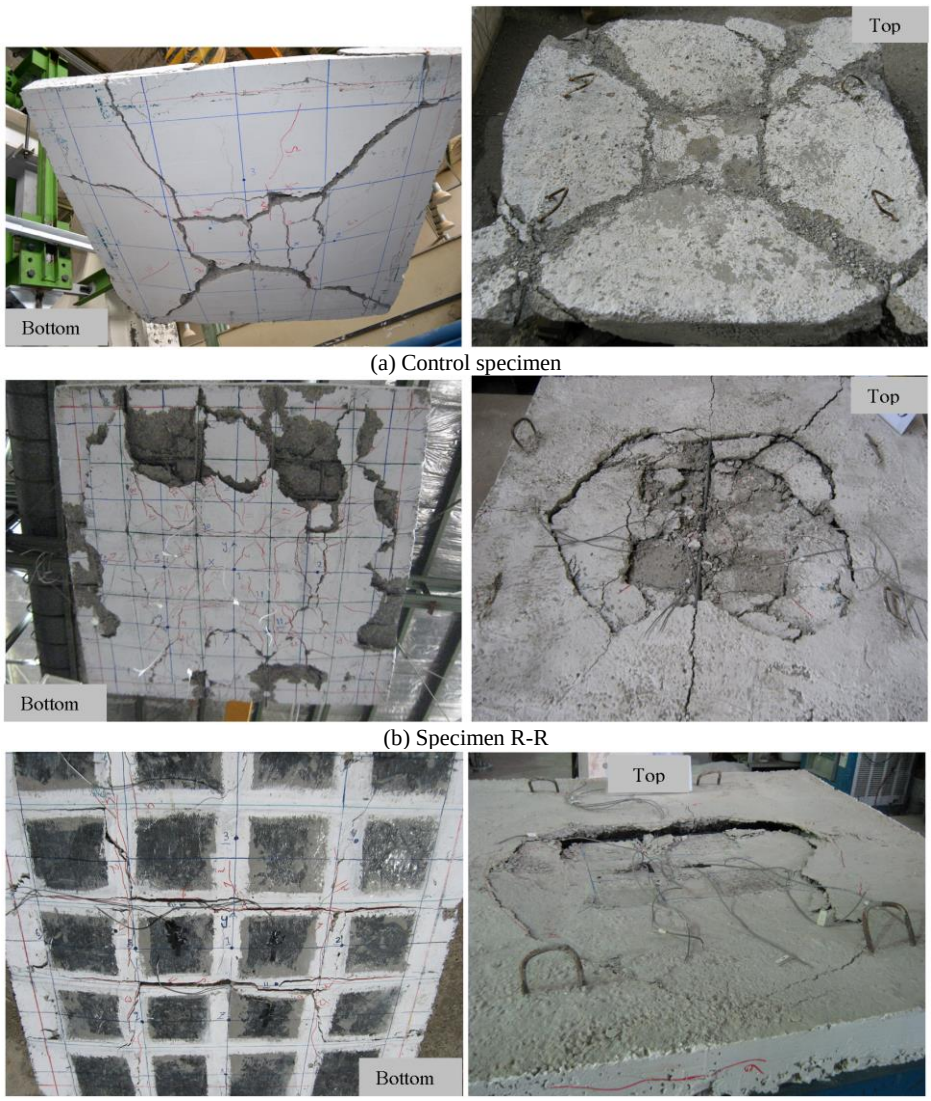

(a) Control specimen

(b) Specimen R-R

(c) Specimen R-F

Figure 8. Cracking patterns of the specimens after failure.

4.5. Steel and concrete strains

Strains were measured on the steel bars and on the concrete compressive face of the slabs. Figure 1 shows the locations of the strain gauges. Load versus steel and concrete strain responses for strain gauges that gave maximum strains are shown respectively in Figures 9 and 10. The vertical line in Figure 9 illustrates the yield strain for steel bars, determined as 2,160 microstrain from uniaxial tension tests. Yielding of the steel bars was observed in all of the specimens. The maximum steel strain measurement for specimens was well above the yield strain (between 15,900 and 18,400 microstrain). The maximum concrete compressive strain reached at the ultimate load of the specimens was about 3,173 microstrain for specimen R-F. This strain level was close to the ultimate uniaxial compressive strain for concrete.

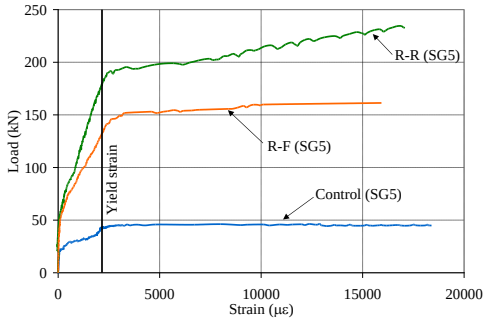

Figure 9. Strain measurements on the steel bars.

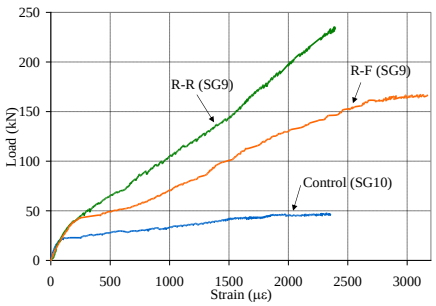

Figure 10. Strain measurements on the concrete compression face of the slabs.

Figure 11 shows the steel strain profiles at Gauges 1 to 5 along the orthogonal axis at the ultimate load of the specimens. The horizontal line in this figure illustrates the yield strain for steel bars (2,160 microstrain). The steel strain versus distance relationship for all specimens had a nonlinear profile. The highest steel strains at all load levels for all specimens were measured by strain Gauge 5 located at the slab center. The lower strains were measured by other strain Gauges located further from the slab center. Initial yielding of steel bars occurred at the slab center and then spread gradually from the center to the edges of the slab. Strengthened specimens had lower steel strain values than the control specimen. Applying the FRP reinforcements reduced the internal steel strains and delayed the onset of failure. Strengthened specimens had steel strain values that ranged from 87 to 93% of those in the control specimen. Although high strain levels in steel bars were reached for strengthened specimens, but the pure flexural failure mode was not reached.

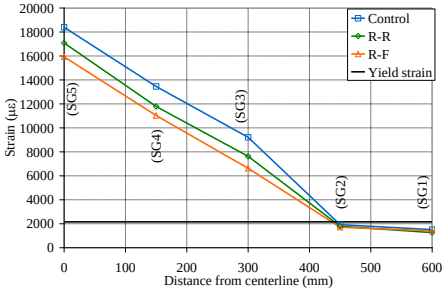

Figure 11. Steel strain profiles at ultimate load.

4.6. FRP strains

Figure 12 shows the load versus the maximum measured FRP reinforcements strain for strengthened specimens. It was observed that FRP strains were small before cracking. After cracking, the FRP reinforcements engaged and started carrying the excessive strains until failure occurred. The maximum strains developed in the GFRP rods and CFRP fabrics were 7,681 and 1,069 microstrain respectively. This corresponds to about 51 and 7% of the ultimate tensile (rupture) strain of the FRP reinforcements, which depended on the slab failure mode and the bond strength between the FRP reinforcements and concrete. In R-F specimen, the strain gauges had been bonded on the unsmooth surface of the EB CFRP fabrics, which resulted in the separation of the gauges from the fabrics surface at high strain levels. As a result, the EB CFRP fabrics showed lower strain values than the NSM GFRP rods.

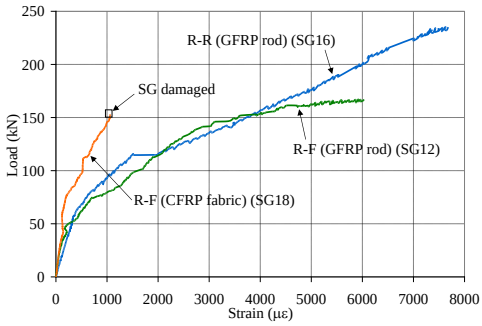

Figure 12. Strain measurements on the FRP reinforcements.

5. Finite element modeling

5.1. Geometry of the developed FE models

Three FE models were developed to simulate the behavior of the full-scale RC slabs, using the FE code ANSYS [17]. The numerical predictions were compared with the experimental results for load-central deflection

response and cracking pattern at failure. The models had the same geometry, dimensions, material properties, loading, and boundary conditions of the experimental tested specimens. Also, the developed FE models had the same notation as those as of the experimental program. One quarter of the slabs was modeled due to the geometrical, loadings, and boundary conditions symmetry. The steel bars and NSM FRP reinforcements was defined as discrete reinforcement model located near the slab tension face. The nodes on the slab compressive face, which correspond to the location of the steel loading plate in the experiment, were coupled in the vertical direction using the constraint equations. Figure 13 shows the general layout of a developed FE model.

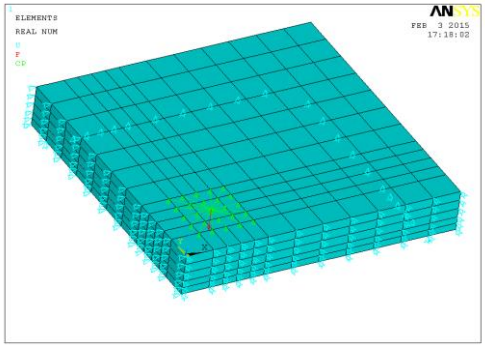

Figure 13. Developed FE model general layout.

5.2. Elements description and material properties

The eight-node structural solid element, SOLID65, was used to model the concrete [17]. Each node of the solid element has three translational degrees of freedom in the x, y, and z directions. The element is capable of plastic deformation, cracking in tension (in three orthogonal directions), and crushing in compression. The 3D two-node structural spar element, LINK8, was used to model the steel bars and NSM GFRP rods [17]. Each node of the element has three translational degrees of freedom. The element is a uni-axial tension-compression element and is capable of plastic deformation. The eight-node layered solid element, SOLID46, was used to model the EB CFRP fabrics [17]. Each node of the element has three translational degrees of freedom. The element allows for up to 100 different material layers with different orientations and orthotropic material properties in each layer. In order to simplify the modeling, the perfect bond between the reinforcements (steel, EB and NSM FRP) and solid concrete elements was assumed by sharing the same nodes.

The william and Warnke [19] failure criterion along with the Drucker-Prager criterion were used to define the constitutive material model for the concrete elements. Drucker-Prager criterion considers the effect of mean normal stress (i.e. confinement) on the yield function and is suitable for modeling the concrete behavior in compression. The behavior of the steel bars was idealized to be bilinear (elastic-plastic) with a post-yield strain hardening of 1% to represent the strain hardening effect of the steel bars. The Von-Misses failure criterion was used to define yielding of the steel bars. The EB and NSM FRP reinforcements were modeled with elastic-brittle behavior (linear stress–strain curve up to brittle failure) in tension and zero strength and stiffness in compression.

5.3. Comparison between FE numerical predictions and experimental results

A comparison was carried out between the FE numerical predictions and experimental results of the load-central deflection response and cracking pattern at failure. Figure 14 compares the load-central deflection responses predicted by FE models with the experimental results for all three slabs. The descending branch of the FE load-central deflection responses was not calculated. As shown in Figure 14, the FE numerical predicted load-central deflection responses agree well with the experimental measurements for all specimens. The load-deflection responses from the FE models were slightly stiffer than those from the experimental results.

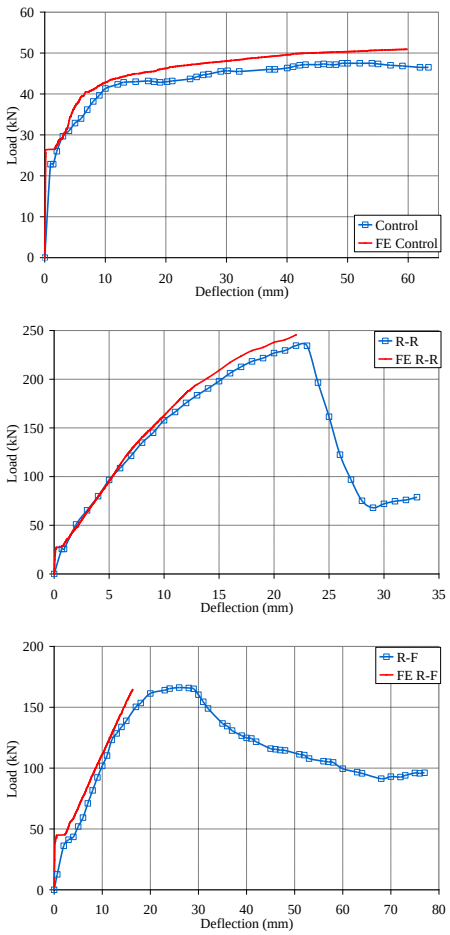

Figure 14. Comparison between FE numerical and experimental results of the load-central deflection response.

Table 4 compares the predicted ultimate loads and deflections of the FE analyses with the tests data. As indicated in Table 4, the maximum deviation between the experimental and predicted numerical results for the ultimate load is less than 7% for all slabs.

Table 4. Comparison between predicted FE numerical and experimental results.

	Exp.		FE		% Difference in P_u
Specimen	P_u (kN)	Δ_u [a] (mm)	P_u (kN)	Δ_u (mm)	(FE–Exp.)/FE
Control	47.50	63.35	50.92	59.79	6.7
R-R	234.50	22.93	245.53	22.06	4.5
R-F	166.17	26.16	164.51	16.33	1.01

[a] Net central deflection at ultimate load carrying capacity.

Figures 15(a-c) show the cracking pattern obtained from the FE analyses at the last converged load step for all models. The black lines in this Figure illustrate the approximate crack pattern for each specimen which were drawn manually along the length of the cracking signs resulted form ANSYS output. For R-F model in Figure 15(c) the EB CFRP fabrics have not been shown. As shown in Figure 15, the cracking pattern from the FE simulations and the actual slabs, reported in Section 4.4., are in reasonably good agreement. It can be concluded that the developed FE models can provide the accurate prediction of the load-central deflection response and cracking pattern at failure for the RC two-way slabs strengthened with FRP reinforcement.

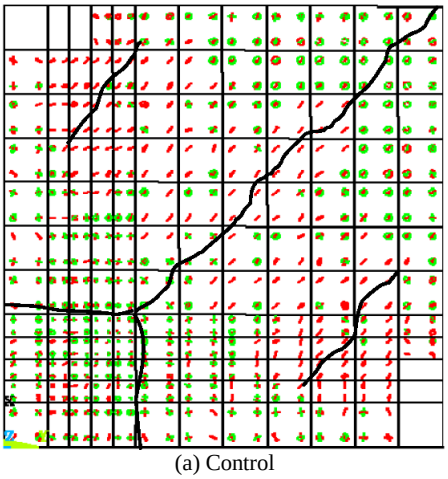

(a) Control

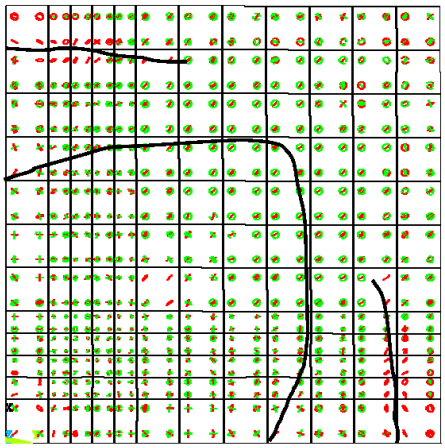

(b) R-R

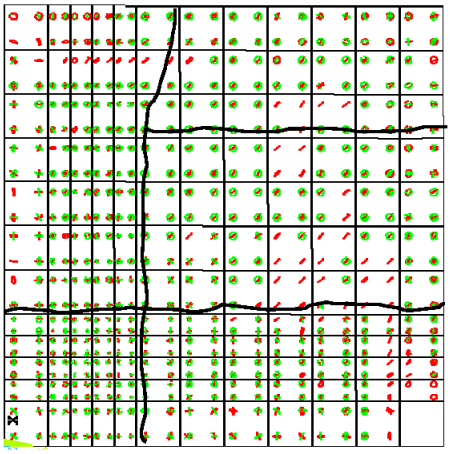

(c) R-F

Figure 15. Cracking pattern of FE models at failure load level.

6. Summary and conclusions

An effective technique based on the combined method for flexural strengthening of existing RC two-way slabs with low clear cover thickness is presented in this study. The proposed strengthening technique employs the use of combination of EB CFRP fabrics and NSM GFRP rods as flexural reinforcements. An experimental program was carried out, and the behavior of the slab strengthened according to this technique was compared to the behavior of the slab strengthened with conventional GFRP rods. A 3D nonlinear simulation was also developed using the FE method and the numerical predictions of load-central deflection response and cracking pattern were compared with the experimental results. The following conclusions can be drawn from this study:

- The test results indicated that the use of the combined FRP technique is feasible and effectiveness technique for improving the flexural behavior of the RC two-way slabs with low clear cover thickness.
- It can be shown that, when the proposed combined FRP technique is used, the grooves can be cut only in one direction of the slab. Therefore, the strengthening of the existing slabs with low clear cover thickness using FRP reinforcements, which was often limited due to the insufficient clear cover thickness in most existing RC slabs and premature debonding failure of the EB FRP reinforcements from the concrete face, can be possible.
- Strengthening of the RC two-way slabs using FRP reinforcements increases their flexural capacity. The specimens R-R and R-F had almost the increase in the flexural capacity of 394 and 250%, respectively, compared with the control specimen. Specimen R-R, strengthened using NSM GFRP rods, showed an increase in ultimate load by 41% over the slab strengthened using combination of EB CFRP fabrics and NSM GFRP rods.
- Strengthened specimens failed in combined flexural and local failure modes due to punching the loading plates through the slab. Failure took place after significant yielding of steel bars. Although high strain levels in steel bars were reached, but the pure flexural failure mode was not reached.
- The strengthened specimens had a stiffer behavior than the control specimen, due to the stiffening effect of FRP reinforcements. Deflection values at the ultimate load of the strengthened specimens were between 38 and 58% of the deflection value of the control specimen.
- The slab strengthened using combination of EB CFRP fabrics and NSM GFRP rods showed higher ductility compared to the slab strengthened using GFRP rods. It was shown that, the increase in flexural capacity was accompanied by a reduction in the ductility of failure.
- The FRP reinforcements reduced the strain in the internal steel bars and resulted in delaying the initiation and controlling propagation of the flexural cracks in slabs.
- There was a reasonably good agreement between the numerical predictions and experimental results in terms of the load-central deflection response and cracking pattern of the specimens.

Acknowledgments

The authors wish to thank Semnan University Science and Technology Park for financial support and colleagues at the University for

technical support. Also they would like to acknowledge PAYA-SAZ-AZHAND Company for providing epoxy adhesives.

References

[1] ACI (American Concrete Institute). (2008). ACI 440.2R-08: "Guide for the design and construction of externally bonded FRP system for strengthening concrete structures". American Concrete Institute, Farmington Hills, MI, USA.

[2] Badawi, M., Soudki, K. (2009). "Flexural strengthening of RC beams with prestressed NSM CFRP rods–experimental and analytical investigation". Constr Build Mater, 23(10), pp.3292-3300.

[3] Anwarul Islam, AKM. (2009). "Effective methods of using CFRP bars in shear strengthening of concrete girders". Eng Struct J, 31, pp.709–714.

[4] De Lorenzis, L., Teng, JG. (2007). "Near-surface mounted FRP reinforcement: An emerging technique for strengthening structure". J Compos Part B Eng, 38(2), pp.119–143.

[5] El-Hacha, R., Riskalla, SH. (2004). "Near-surface-mounted fiber-reinforced polymer reinforcements for flexural strengthening of concrete structures". ACI Struct J, 101(5), pp.717–726.

[6] Barros, JAO., Dias, SJE., Lima, JLT. (2007). "Efficacy of CFRP-based techniques for the flexural and shear strengthening of concrete beams". J Cem Concr Compos, 29(3), pp.203–217.

[7] Ceroni, F. (2010). "Experimental performances of RC beams strengthened with FRP materials". Constr Build Mater, 24(9) , pp.1547-1559.

[8] Jalali, M., Sharbatdar, MK., Chen, JF., Jandaghi Alaee, F. (2012). "Shear strengthening of RC beams using innovative manually made NSM FRP bars". Constr Build Mater, 36, pp.990–1000.

[9] Barros, JAO., Baghi, H., Dias, SJE., Gouveia, AV. (2013). "A FEM-based model to predict the behaviour of RC beams shear strengthened according to the NSM technique". Eng Struct J, 56, pp.1192–1206.

[10] Sharaky, IA., Torres, L., Comas, J., Barris, C. (2014). "Flexural response of reinforced concrete (RC) beams strengthened with near surface mounted (NSM) fibre reinforced polymer (FRP) bars". Compos Struct J, 109, pp.8–22.

[11] Bonaldo, E., Barros, JAO., Lourenco, PB. (2008). "Efficient strengthening technique to increase the flexural resistance of existing RC slabs". J Compos Constr, 12(2), pp.149–159.

[12] Elgabbas, F., El-Ghandour, AA., Abdelrahman, AA., El-Dieb, AS. (2010). "Different CFRP strengthening techniques for prestressed hollow core concrete slabs: Experimental study and analytical investigation". Compos Struct J, 92, pp.401–411.

[13] Dalfré, GM., Barros, JAO. (2013). "NSM technique to increase the load carrying capacity of continuous RC slabs". Eng Struct J, 56, pp.137–153.

[14] Mostakhdemin Hosseini, MR., Dias, SJE., Barros, JAO. (2014). "Effectiveness of prestressed NSM CFRP laminates for the flexural strengthening of RC slabs". Compos Struct J, 111, pp.249–258.

[15] Breveglieri, M., Barros, JAO., Dalfré, GM., Aprile, A. (2012). "A parametric study on the effectiveness of the NSM technique for the flexural strengthening of continuous RC slabs". Compos Part B Eng, 43(4), pp.1970–1987.

[16] Foret, G., Limam, O. (2008). "Experimental and numerical analysis of RC two-way slabs strengthened with NSM CFRP rods". Constr Build Mater, 22(10), pp.2025–2030.

[17] ANSYS – release version 11. (2007). "A finite element computer software theory and user manual for nonlinear structural analysis". ANSYS 2007, Inc. Canonsburg, PA.

[18] ACI (American Concrete Institute). (1999). ACI 318-99: "Building code requirements for structural concrete, American Concrete Institute". Farmington Hills, MI, USA.

[19] William, KJ., Warnke, EP. (1975). "Constitutive model for the triaxial behavior of concrete". IABSE Proc., Int. association for bridge and structural engineering, Zürich, 19, pp.174.